AGU PUBLICATIONS

JGR

Journal of Geophysical Research: Oceans

RESEARCH ARTICLE

10.1002/2015JC011107

Key Points:
- Multivariate wave climate time series preserving seasonality, interannual variability and chronology
- Future wave climate time series accounting for possible changes in the global climate system
- Long-term (decades) morphodynamic simulations

Supporting Information:
- Supporting Information S1

Correspondence to:
J. A. A. Antolínez,
aantolinezja@unican.es

Citation:
Antolínez, J. A. A., F. J. Méndez, P. Camus, S. Vitousek, E. M. González, P. Ruggiero, and P. Barnard (2016), A multiscale climate emulator for long-term morphodynamics (MUSCLE-morpho), *J. Geophys. Res. Oceans*, *121*, 775–791, doi:10.1002/2015JC011107.

Received 8 JUL 2015
Accepted 18 DEC 2015
Accepted article online 22 DEC 2015
Published online 22 JAN 2016
Corrected 2 FEB 2016

This article was corrected on 2 FEB 2016. See the end of the full text for details.

A multiscale climate emulator for long-term morphodynamics (MUSCLE-morpho)

José Antonio A. Antolínez[1], Fernando J. Méndez[1], Paula Camus[1], Sean Vitousek[2], E. Mauricio González[1], Peter Ruggiero[3], and Patrick Barnard[2]

[1]Environmental Hydraulics Institute "IH Cantabria", Universidad de Cantabria, Santander, Cantabria, Spain, [2]Pacific Coastal and Marine Science Center, United States Geological Survey, Santa Cruz, California, USA, [3]College of Earth, Ocean, and Atmospheric Sciences, Oregon State University, Corvallis, Oregon, USA

Abstract Interest in understanding long-term coastal morphodynamics has recently increased as climate change impacts become perceptible and accelerated. Multiscale, behavior-oriented and process-based models, or hybrids of the two, are typically applied with deterministic approaches which require considerable computational effort. In order to reduce the computational cost of modeling large spatial and temporal scales, input reduction and morphological acceleration techniques have been developed. Here we introduce a general framework for reducing dimensionality of wave-driver inputs to morphodynamic models. The proposed framework seeks to account for dependencies with global atmospheric circulation fields and deals simultaneously with seasonality, interannual variability, long-term trends, and autocorrelation of wave height, wave period, and wave direction. The model is also able to reproduce future wave climate time series accounting for possible changes in the global climate system. An application of long-term shoreline evolution is presented by comparing the performance of the real and the simulated wave climate using a one-line model.

1 Introduction

Over millennia, Earths' climate has been continuously oscillating. These changes are reflected in the ocean's extent (sea-level), contents (distribution of heat and salt), and behavior (wave climate and circulation patterns); and consequently their impacts to the coast. Approximately 10% of the world population lives in the coastal zone below 10 m elevation [*Nicholls and Cazenave*, 2010], and it is thought that climate cycles have motivated humans to relocate throughout history [*Griggs*, 2013]. The latest *IPCC* [2013] report confirms that climate change is unequivocal, as evidenced by unprecedented, over decades to millennia: warming of the atmosphere and the ocean, diminishing ice sheets and rising sea levels. Motivated by anticipated changes in sea level and wave climate, coastal researchers have increased their interest in understanding long-term morphodynamic evolution [*Elko et al.*, 2014]. Nevertheless, understanding and modeling long-term behavior remains a significant challenge. Many modeling techniques exist to simulate long-term coastal change. Process-based numerical models tend to induce discretization errors and typically require high computational efforts. In order to reduce computational cost, several acceleration techniques have been developed including model reduction, input reduction, and behavior-oriented techniques [*de Vriend et al.*, 1993a,1993b]. In this paper, we provide a novel input reduction technique for wave-driven, long-term morphodynamic modeling. Many input reduction techniques exist, like the Multiple Representative Wave (MRW) approach [*Steijn*, 1992], and the Simple Representative Wave (SRW) approach [*Chesher* and *Miles*, 1992], which seek to reconstruct the measured wave forcing. *Southgate* [1995] demonstrated the importance of accounting for the wave chronology. *Chonwattana et al.* [2005] proposed an improved method that conserves wave energy flux. Recently, *Walstra et al.* [2013] show how to maintain the frequency of occurrence and the chronology of the original wave time series. To simulate the long-term effects of tide, *Latteux* [1995] introduced an approach to represent the whole tidal cycle using only a small number of tidal constituents. Several input-reduction techniques are integral to the long-term morphology models proposed by *Roelvink* [2006]. Examples of the application of these techniques include *Lesser* [2009] and the hybrid model of [*Zhang et al.*, 2004]. As an alternative to deterministic long-term predictions, *Callaghan et al.* [2008, 2013] proposed use of probabilistic techniques.

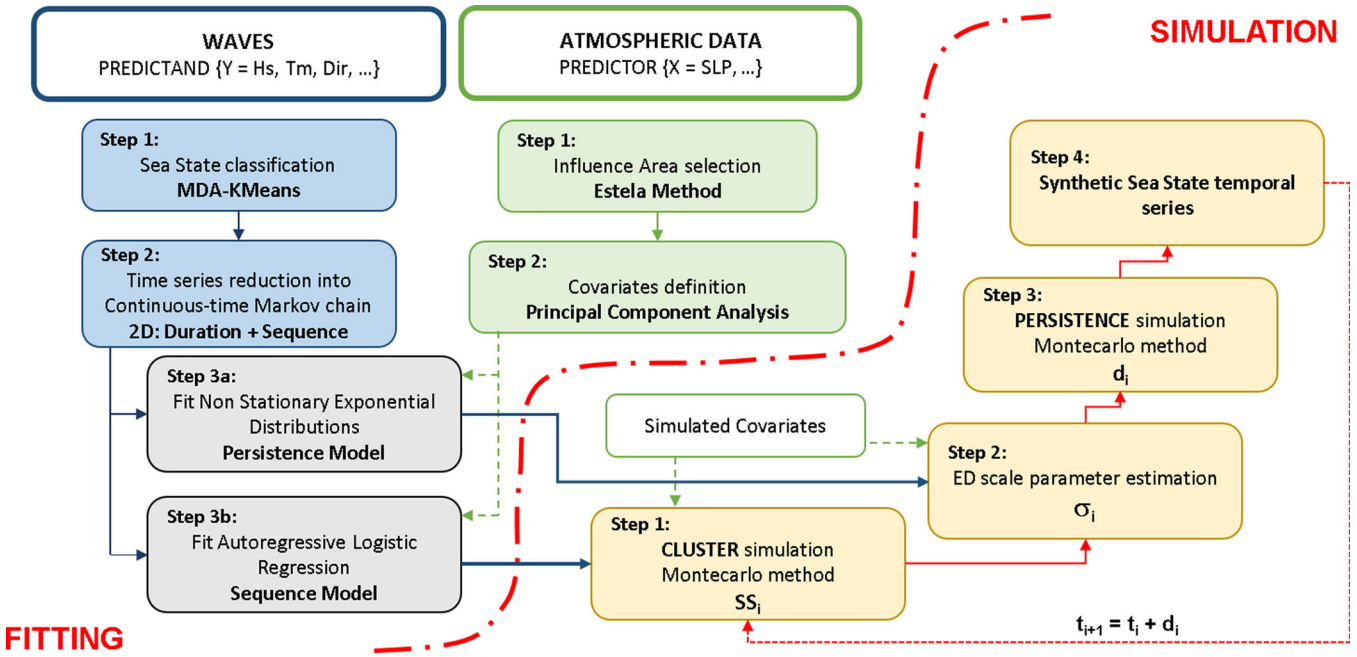

Figure 1. Diagram of the model fitting and simulation.

In order to incorporate climate change, large-scale and long-term morphodynamics studies require accurate forcing definition in terms of wave-driver behavior and evolution [*Kaergaard and Fredsoe*, 2013]. In this paper, we focus on methods to provide a reduced wave input time series, which is often considered the main driver of coastal evolution. The method maintains the chronology of the wave conditions, a key component in morphodynamics [*de Vriend et al*., 1993a; *Walstra et al*., 2013], but also in estimating the probability of structural failure of offshore platforms [*Salvadori et al*., 2014] and vertical breakwaters [*Gōda*, 2010]. Even for different drivers than waves, e.g., wind, methods that retain the temporal evolution of the forcing can be crucial, like in the computation of fatigue loads in wind turbines [*Thomsen and Sørensen*, 1999]. Furthermore, in a changing climate, we need to understand any climate-controlled driver dependencies. The main goal of this research is to introduce a general framework for reducing dimensionality of wave input, taking into account global atmospheric circulation fields and dealing simultaneously with seasonality, interannual variability, long-term trends, and autocorrelation of wave height, wave period, and wave direction. Evolution in these dependencies will result in changes in the wave climate driver behavior.

In this paper, the multiscale climate emulator for long-term morphodynamics (MUSCLE-morpho) is presented. The paper is organized as a sequence of successive steps to be performed (see Figure 1). Below, section 2 describes the location where the model is applied and the data used in the model. Next, section 3 explains the initialization of the MUSCLE-morpho model and section 4 presents the validation of the model and an example of application for long-term mophological evolution. Finally, the conclusions of this paper are presented in section 5.

2. Data

The proposed methods are applied to the Northwest coast of Spain (lon = 9.25°W and lat = 43.5°N, WGS84 global reference coordinate system). The North Atlantic coast experiences significant wave heights ranging from 1–8 m, mean periods of 6–12 s, and mean direction from the Northwest at approximately 280°–300°. Although we focus here on the North Atlantic, the methods presented are applicable to a wide range of geographic settings.

2.1. Predictor Characterization

Surface winds are the primary driver of ocean waves. However, in global circulation models, near-surface wind fields are not as well reproduced as sea-level pressure fields [*Caires et al*., 2006]. Furthermore, wind

fields can be diagnosed from sea-level pressure fields. Specifically, the geostrophic wind direction is well-represented by isobars and geostrophic wind speed is proportional to pressure gradients. Therefore, sea-level pressure fields and the square of sea-level pressure gradients define the wave predictor indices. This approach is in line with the downscaling statistical predictor used by *Wang et al*. [2012], *Casas-Prat et al*. [2014], and *Camus et al*. [2014a]. In this work, we use the Sea Level Pressure (SLP) fields of the NCEP/NCAR reanalysis-I [*Kalnay et al*., 1996] from the National Center for Environmental Prediction-National Center for Atmospheric Research. The SLP data from NCEP-NCAR reanalysis-I used in this work consist of 6 hourly fields on a 2.5° by 2.5° grid.

2.2. Predictand Characterization

Historical data on the local wave climate predictand are required in the MUSCLE-morpho model. The historical wave information used in this work is the ocean wave reanalysis database Global Ocean Waves (GOW) [*Reguero et al*., 2012]. Here we use waves from a GOW regional simulation over the European Atlantic area, which spans from 27.25°N to 57.25°N and 20°W to 37°E with a spatial resolution of 0.25°. The European Atlantic domain is forced with wind fields from SeaWind I, a dynamic atmospheric downscaling from NCEP-NCAR reanalysis-I [*Menendez et al*., 2013]. This model provides hourly sea-state parameters (significant wave height, mean period, peak period, and mean wave direction) from 1948 to 2014. Because of inhomogeneities in NCEP/NCAR reanalysis prior to 1957 [*Kistler et al*., 2001], the time period covered by this research is from 1960 to 2013. Data from 1960 to 1989 (30 years) is selected to perform the model fit, and data from 1990 to 2013 (24 years) covers the validation period.

3. Model Fit

Below we describe the procedure for establishing a reduced-dimensionality, multivariate sea-state time series. The procedure attempts to take into account dependencies from global atmospheric circulation fields and deals simultaneously with seasonality, interannual variability, long-term trends, and autocorrelation of the trivariate sea state parameters (wave height, period, and direction). As shown in Figure 1, the procedure is divided into two phases, one concerning the definition of the predictor, and the other concerning the definition of the predictand and its relationship to the predictor.

3.1. Predictor Fit

In section 2.1, SLP fields and square SLP gradients have been defined as the predictor of the wave data for the study site. The predictor data is processed in two steps, described below.

3.1.1. Step 1: ESTELA Method

To extract the recent and past atmospheric conditions with daily resolution (daily mean SLP fields and square SLP gradients) over the North Atlantic basin, the ESTELA method of *Pérez et al*. [2014a, 2014b] is applied. The ESTELA method evaluates the source and travel time of wave energy reaching a local area. Thus, following the methodology proposed by *Camus et al*. [2014b], a dynamic predictor is defined by a local component which represents short-wave-period seas and a regional one which represents long-period swell. A local area (green rectangle in Figure 2) covering latitude from 40°N to 50°N and longitude from 20°W to 5°W with 1 day of temporal coverage (the same as the wave record) and a regional area covering latitude from 35°N to 70°N and longitude from 60°W to 5°W with 4 days of temporal coverage (the wave record day and three previous days) are defined to extract the recent and past atmospheric conditions with daily resolution (daily mean SLP fields and square SLP gradients) in these areas over the North Atlantic basin.

3.1.2. Step 2: Principal Component Analysis

A Principal Component Analysis (PCA) is then applied to the SLP fields to obtain the dominant spatial variability patterns (EOFs) and their corresponding temporal coefficients (PCs). To reduce the dimensionality of the temporal SLP fields while preserving the maximum variance of the sample data, the first 36 modes from the PCA analysis (explaining 95% of the variance) are selected as the predictor of the wave data in the Atlantic basin. As an example, the covariate associated to the first mode is mathematically expressed as $PC_1(t)$, where t is time. The PCs are the covariates for both models fitted below.

Figure 2 shows the first four EOFs and the corresponding PCs ($PC_1(t)$, $PC_2(t)$, $PC_3(t)$ and $PC_4(t)$) of the predictor, the PCs are standarized and the EOFs multiplied by the corresponding standard deviation for easy comparison. The EOFs are defined by the anomalies of SLP and squared SLP gradients in the generation and local areas. The SLP anomalies are represented by contour lines, with positive anomalies in red and negative

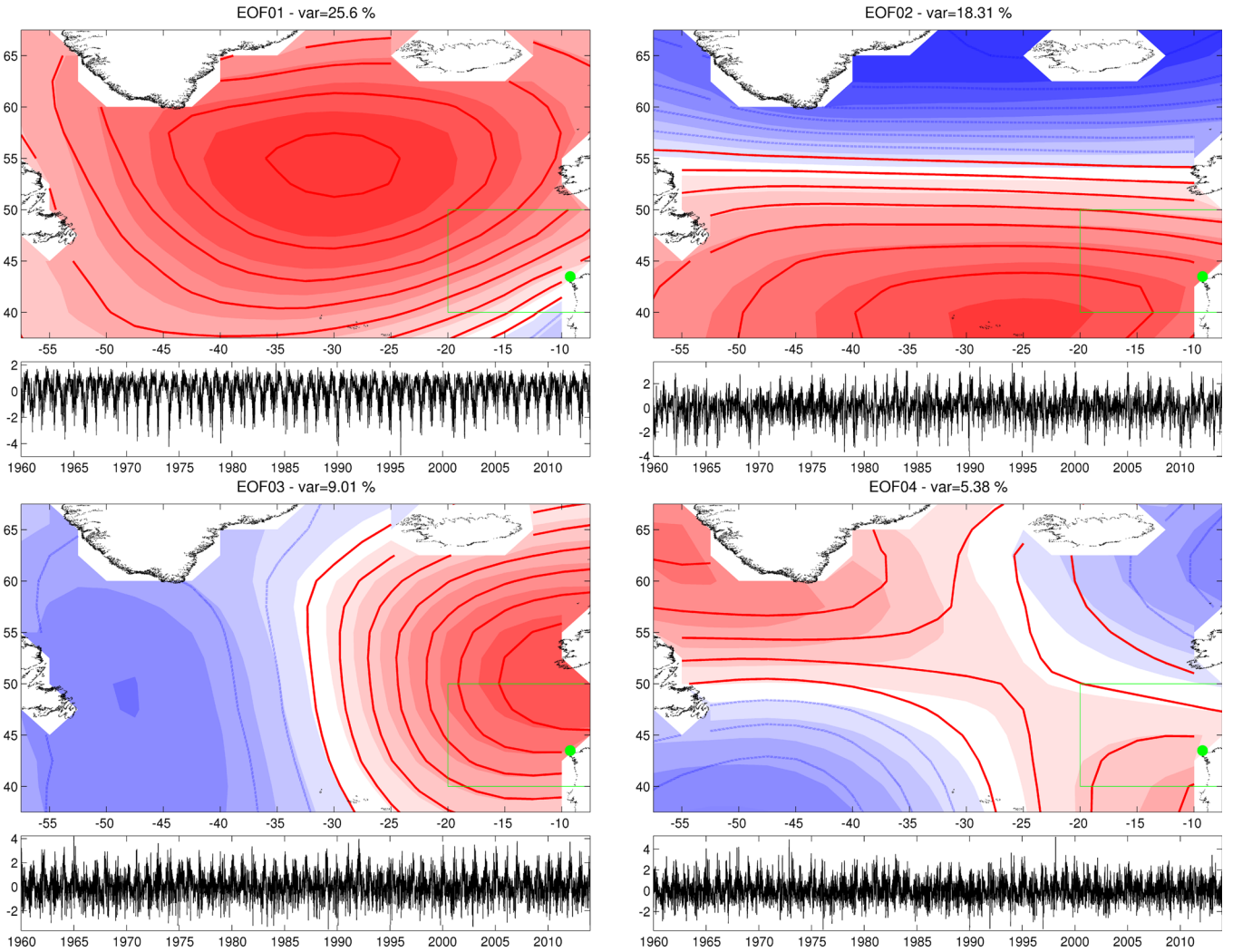

Figure 2. The first four empirical orthogonal functions (EOFs) and principal components (PCs) of the predictor (SLP). The SLP anomalies are represented by contour lines, with positive anomalies in red and the negative anomalies in blue. The anomalies of the squared SLP gradients are represented with blue-white-red scale. The green point represents the study site, and the green polygon represents the local area for the predictor.

anomalies in blue. Note that in the case of the regional area, the land points are not considered in the predictor definition, but they are considered in the local area.

3.2. Predictand Fit

The homogeneous, continuous, and calibrated time series of multivariate wave climate described in section 2.2 representing the predictand in the MUSCLE-morpho model is transformed into a Continuous-time Markov chain [*Norris*, 1997a,1997b] in three steps.

3.2.1. Step 1: Sea State Classification

In the first step of the predictand fit, the multivariate continuous time series is categorized into discrete sea states by classification techniques. Following *Camus et al.* [2011], the K-means algorithm technique (KMA) is applied to multivariate time series of wave height, period, and direction. The maximum dissimilarity algorithm (MDA) is applied as a centroid initialization technique to force the KMA technique to correctly describe the diversity of the wave climate [*Camus et al.*, 2011]. This method is applied to the GOW multivariate data set from 1960 to 1989, to obtain $N = 16$ sea states clusters. We note that 16 clusters are selected (i) for the sake of simplicity, (ii) to facilitate implementation, fit, and interpretation of the model results and (iii) to reduce computational effort. The classification produced by the KMA algorithm applied to the predictand data is shown in Figure 3. The black and colored points represent the centroids and classes of the predictand data, respectively.

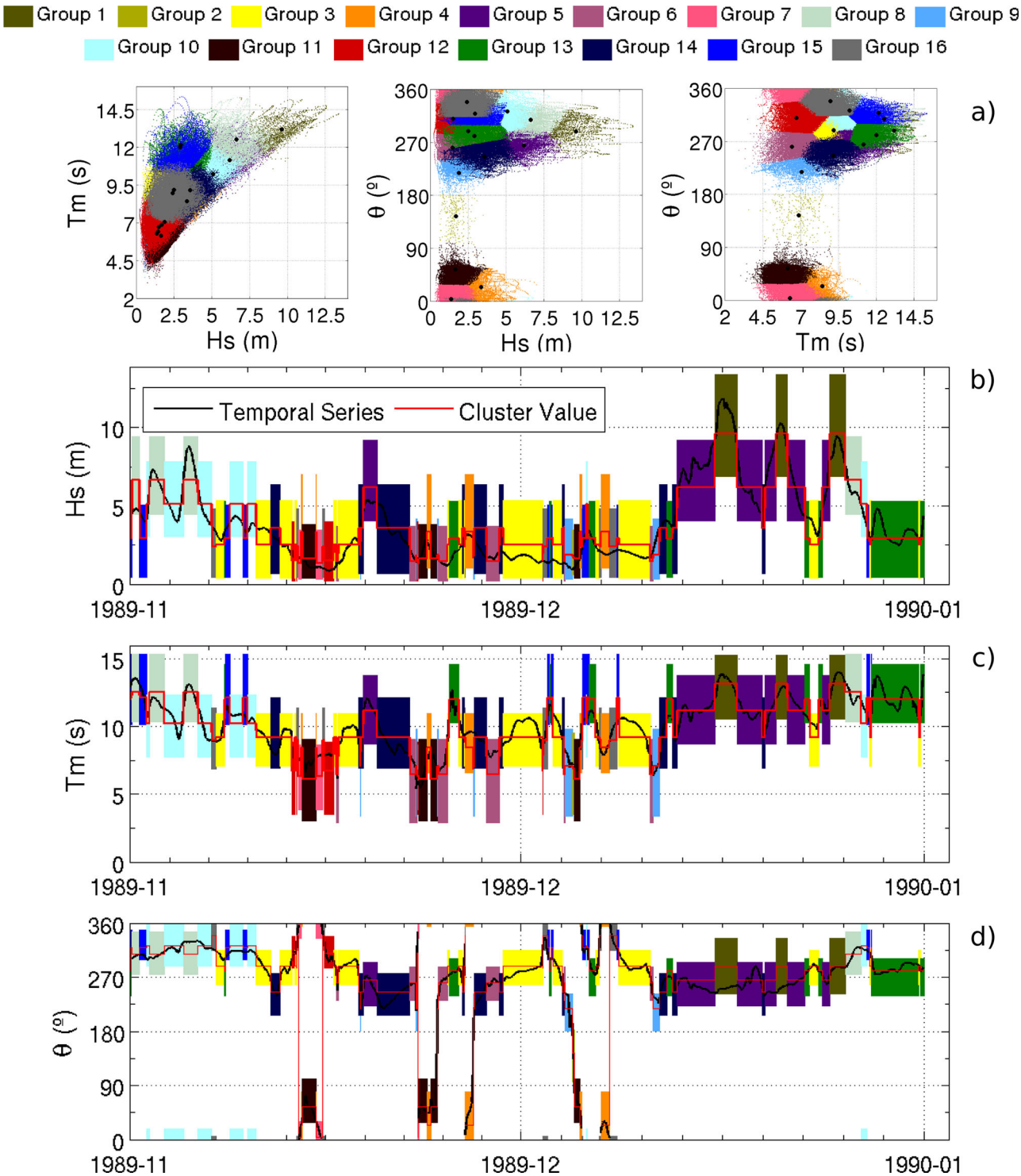

Figure 3. (a) Multivariate classification and time series of (b) wave height, (c) period, and (d) direction reduced in terms of cluster sequencing and duration. The different colored bins represent the different clusters. The width of the bins represents the duration within each cluster, and the height of the bin represents the minimum and maximum value taken for each variable of the multivariate wave climate.

3.2.2. Step 2: Time Series Reduction

Once the classification is obtained, each hourly record of wave height, period, and direction belongs to one of the 16 clusters namely, Sea States (SS). Subsequently, the hourly data are categorized in terms of event sequence and duration. The event sequence time series represents the evolution (ordering) in time of the SSs.

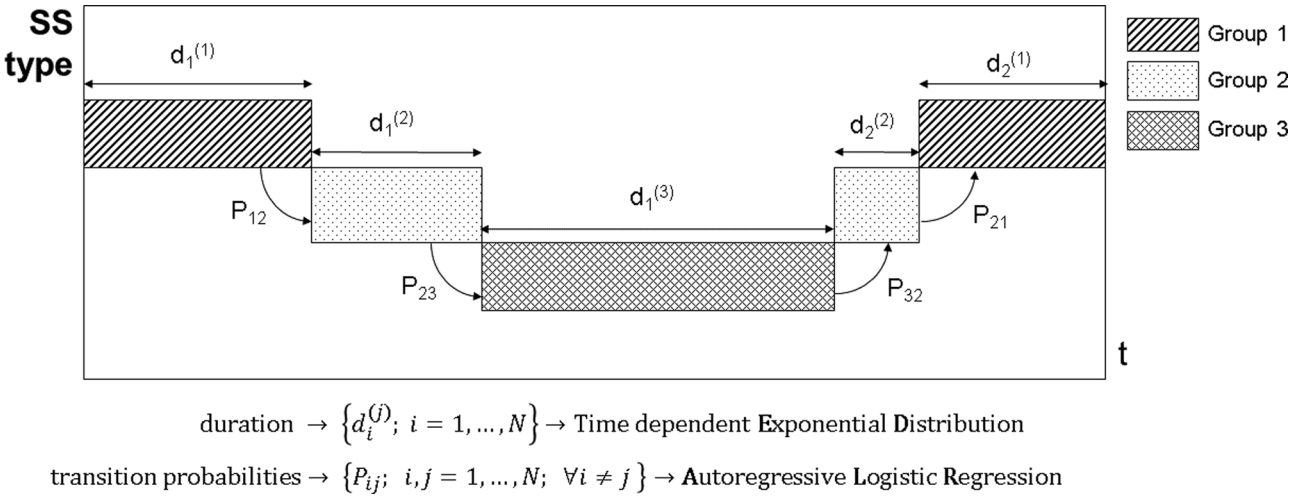

$$\text{duration} \rightarrow \left\{d_i^{(j)};\ i = 1, \ldots, N\right\} \rightarrow \text{Time dependent Exponential Distribution}$$

$$\text{transition probabilities} \rightarrow \left\{P_{ij};\ \ i, j = 1, \ldots, N;\ \ \forall i \neq j\right\} \rightarrow \text{Autoregressive Logistic Regression}$$

Figure 4. Reduction of the multivariate time series into a continuous-time Markov chain as proposed by *Norris* [1997a,1997b].

The duration time series represents the persistence of each SS. The projection of the multidimensional initial data (regardless of the size) into event sequence and duration time series using classification techniques seeks to preserve the (i) probability of being within a particular SS for a duration d and (ii) the probability of changing between one SS n_i to another n_j. In step 3, models for both duration and event sequence are obtained including any global atmospheric pattern, seasonality, interannual variability, long-term trends, and autocorrelation relationships in their definition. An integer value between $n = 1$ and $n = 16$ is arbitrarily assigned to each SS, as in Figure 3, resulting in (i) the sequence of SS, which is modeled with a time-dependent logistic model, and (ii) the sequence of persistence for each SS, which is modeled with a time-dependent exponential distribution. This procedure reduces the multivariate time series to a bidimensional data set in SS sequence and persistence space as shown in Figure 4.

3.2.3. Step 3a: Persistence Model

In this section, we describe the procedure to obtain the persistence model. We fit a regression model for each SS cluster based on a time-dependent Exponential Distribution (ED). The lone scale parameter σ_t, is obtained using pseudo-optimal selection techniques following *Mínguez et al*. [2010]. SS persistence records are assumed to be independent random variables. The persistence D_t of each cluster n_j at time t follows an ED with a time-dependent scale parameter σ_t, and a probability density function (PDF) given by:

$$g(d_t; \sigma_t) = \frac{1}{\sigma_t} e^{-\frac{d_t}{\sigma_t}} \tag{1}$$

Note that D_t is the random variable associated with the persistence of a particular cluster at time t and d_t is a particular value or data of the corresponding random variable. To introduce seasonality, long-term trends and the influence of different covariates (predictor indices defined in section 3.1), the model proposed by *Menéndez et al*. [2009] and *Mínguez et al*. [2010] is formulated for the scale parameter as follows:

$$\log(\sigma_t) = \alpha_0 + \sum_{i=1}^{P_\sigma} \left[\alpha_{2i-1} \cos(i\omega t) + \alpha_{2i} \sin(i\omega t)\right] + \alpha_{LT} t + \sum_{k=1}^{Q_\sigma} \alpha_k^{co} PC_k(t) \tag{2}$$

where t is given in years, $\log(\sigma_t)$ ensures positivity of the scale parameter ($\sigma_t > 0$), α_0 is the mean value, α_i are the harmonic amplitudes, $\omega = 2\pi/T$ is the angular frequency, T is a period of one year, and P_σ is the number of sinusoidal harmonics to be considered within the year, α_{LT} and α_k^{co} are the coefficients of the long-term trends and covariates, respectively, Q_σ is the number of covariates considered, and $PC_k(t)$ is the value of covariate k at time t.

The parameters are estimated maximizing the likelihood function and the optimal combination of parameters is obtained minimizing the Akaike Information Criteria (see details in *Mínguez et al*. [2010]). (Supporting information Table S1file shows the optimal coefficients obtained for each SS.)

3.2.4. Step 3b: Sequence Model

Step 3b consist of modeling the SS sequence using an autoregressive logistic model (ALR) that allows the simulation of synthetic sequences of SSs while taking into account different covariates such as seasonality, predictor indices ($PC_k(t)$ defined in section 3.1) and autoregressive terms. Appropriately modeling SS sequence is important because it is known that sea conditions at any given point in time depend on the previous conditions and may be affected by atmospheric behavior of both the present and previous days. Moreover, the qualitative response of the ALR model is useful when working with classified data. Further information related to the theoretical foundation and covariate implementation can be found in *Guanche et al*. [2013]. Here, the fitting process is described briefly.

Let $Y_t; t=1;\ldots;N$ be the observations of SS at time t, with the following possible outcomes $Y_t \in \{1,\ldots,n_{ss}\}$ related to each SS. Considering $X_t; t=1;\ldots;N$ to be a time-dependent row vector of covariates with dimensions $(1\times n_c)$ (i.e., seasonal cycle, principal components $PC_k(t)$ of synoptic circulation, long-term trend, etc.), the autoregressive logistic model is stated as follows:

$$\begin{aligned}&\text{Prob}\,(Y_t=i|Y_{t-1},\ldots,Y_{t-e},X_t)=\\&=\frac{\exp(\beta_{0,i}+\beta_{1,i}\cos\omega t+\beta_{2,i}\sin\omega t+\sum_{j=1}^{n_{pc}}\beta_{j,i}^{PC}PC_j(t)+\beta_i^{LT}t+\sum_{j=1}^{e}Y_{t-j}\gamma_{j,i})}{\sum_{k=1}^{n_{ss}}\exp(\beta_{0,k}+\beta_{1,k}\cos\omega t+\beta_{2,k}\sin\omega t+\sum_{j=1}^{n_{pc}}\beta_{j,k}^{PC}PC_j(t)+\beta_k^{LT}t+\sum_{j=1}^{e}Y_{t-j}\gamma_{j,k})};\\&\forall i=1,\ldots,n_{ss}\end{aligned}\tag{3}$$

where t is given in years, $\beta_{0,i}$ correspond to annual mean values, and $\beta_{1,i}$ and $\beta_{2,i}$ are the harmonic amplitudes. $PC_j(t)$ are row vectors of the n_{pc} different covariates, and $\beta_{j,i}^{PC}$ is the corresponding parameter vector. β_i^{LT} represents the long-term trend effects. Y_{t-j} is the SS of the previous j-states, $\gamma_{j,i}$ is the parameter associated with previous j-state, and the order e corresponds to the number of previous states that influence the actual SS.

Parameter estimation is performed using the maximum likelihood estimator, which requires the definition of the likelihood function. The criteria to choose the final model, i.e., the order of the auto-regressive components, seasonality, number of predictor indices, etc., are based on statistical significance, in particular, the likelihood ratio (LR) statistic (see details in *Guanche et al*. [2013]).

The model includes terms representing harmonics, covariates, and a second-order Markov Chain. (The coefficients for the different terms in (3) are presented for each SS in supporting information Table S2 file.)

4. Model Simulation/Validation

Once the fitting process is completed, the model allows for the simulation of categorical synthetic time series of SSs (like a continuous-time Markov chain; *Norris* [1997a,1997b]). Note that the model can be performed as: (i) an input reduction technique, allowing for the generation of synthetic series of SSs representative of past wave climate characteristics. (ii) A model of future SS time series including changes in global climate system, and thus changes in magnitude, frequency, persistence, and event sequence of the wave climate. Figure 1 shows the procedure to simulate nominal synthetic series of SSs in the two cases above. We describe these methods in the following two sections, one for the predictor simulation and the other for the predictand simulation.

4.1. Predictor Simulation

While the purpose of this research is not to define a new methodology for simulating predictor variables, it is important to mention the works in this field of *Guanche et al*. [2013] for inferring daily covariate indices from monthly sea level pressure fields, *Pérez et al*. [2014, 2015] for computing future regional multimodel projections of surface variables driven by the atmospheric circulation (from the different global climate models, GCMs) based on weather types and statistical downscaling. For reducing uncertainty in temporal series of SS predictions, historical SLP fields, preprocessed as in section 3.1, are used as predictor covariates in the simulation model.

4.2. Predictand Simulation

Step 1 of the predictand simulation procedure involves selecting a SS cluster at time t_i. This is computed, by first obtaining occurrence probabilities of each cluster Y from the ALR model at time t_i with n_c covariates (simulated PCs) considered and e previous SSs. Formally, the categorical distribution that is the generalization of

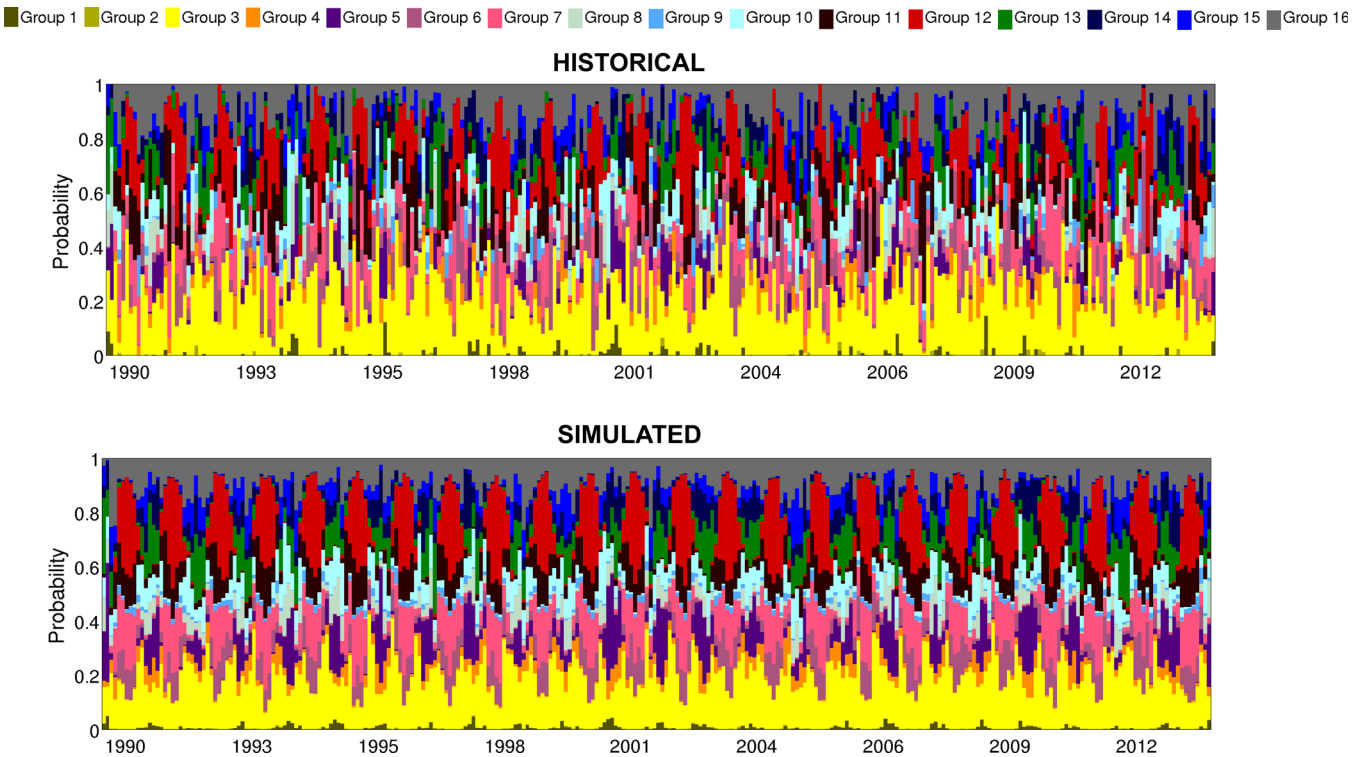

Figure 5. Monthly probability of occurrence of each SS for the validation period, for the (top) historical and (bottom) synthetic series. Interannual variations along years are also shown in this plot, as those presented in the group 10. In the synthetic series, the variability is smoothed because it represents the mean value of the 100 simulations.

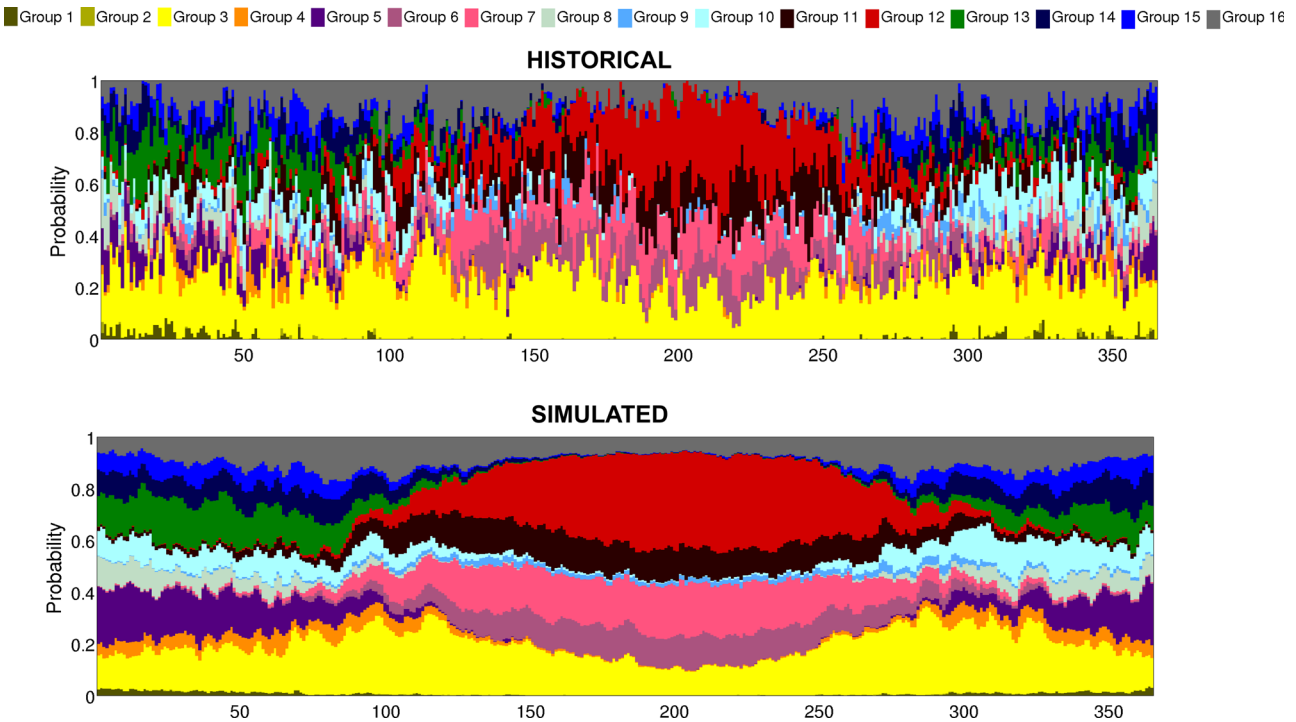

Figure 6. Daily probability of occurrence of each SS for an average year over the validation period for the (top) historical and (bottom) synthetic series. The variability presented in the simulated series differs from the historical one because it represents the mean value of the 100 simulations.

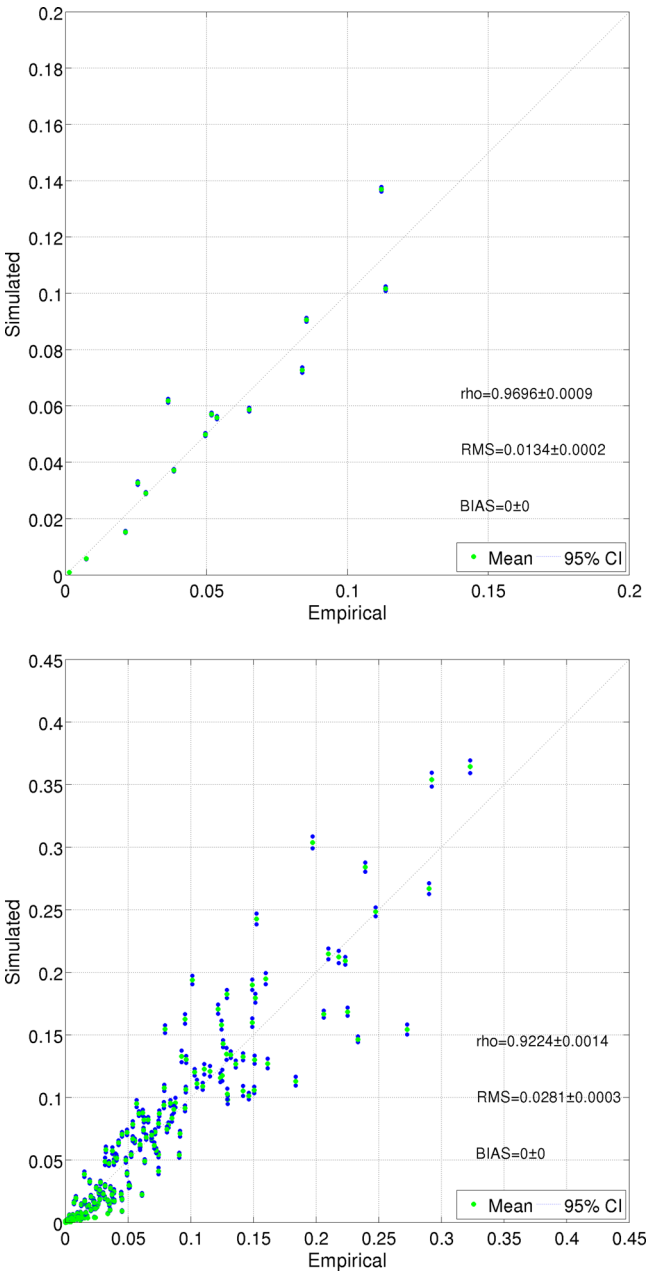

Figure 7. Comparison between historical (*x* axis) and simulated (*y* axis) (top) total occurrence probability of each cluster and (bottom) monthly occurrence probability for each cluster. Green dots represent mean values, and blue ones represent 95% confidence intervals.

the Bernoulli distribution for a qualitative random variable is obtained at time t_i from the ALR model. The parameters specifying the probabilities of each possible outcome are constrained only by the fact that each probability must be in the range 0 to 1, and all must sum to 1. Thereby the corresponding SS at time t_i from the cumulative probabilities of the categorical distribution is selected applying a simple Monte Carlo (MC) method. *Step 2* models the persistence in the current SS n_i. The scale parameter of the ED at time t_i for cluster n_i is obtained accordingly to (2) with Q_σ covariates. This allows the generation of probabilities based on an Exponential Distribution (ED), used in *Step 3* for obtaining the persistence d_i of cluster n_i at time t_i. The persistence value d_i is again obtained by correlating cumulative ED probability of persistence with a random number in [0,1] from a simple Monte Carlo (MC) method. In *Step 4*, the synthetic time series of SSs is constructed from the cluster and persistence values obtained in the previous steps, and a new time instance $t_{i+1}=t_i+d_i$ is calculated. These steps (1–4) are repeated until the synthetic time series of intended length is completed.

Here, the procedure described above is applied for the years 1990–2013 to validate the methodology. The simulation (see Figure 1) is repeated 100 times and 95% confidence intervals are given with results. The initialization of each simulation requires the assumption of a number of previous SSs for the Autoregressive term of the ALR model. In this case, the previous $e=2$ SSs have been taken because of the highest autoregressive term in the best sequence model has order 2.

4.3. Validation

In this section, results are discussed to validate the prediction capabilities of the model for the Northwest coast of Spain. This validation is performed by comparing the results of the simulations with historical data. In this validation, we compare: (i) probability of occurrence of each SS, (ii) probability of transfer between SSs, (iii) mean wave energy flux, (iv) mean wave energy flux direction and (v) modeled shoreline evolution. Additionally, several temporal scales (i) concerning the interannual, (ii) seasonal, and (iii) daily behavior are analyzed. The agreement between the simulated and historical data is computed with the correlation coefficient (ρ), the root mean square error (*RMS*), and the *bias*.

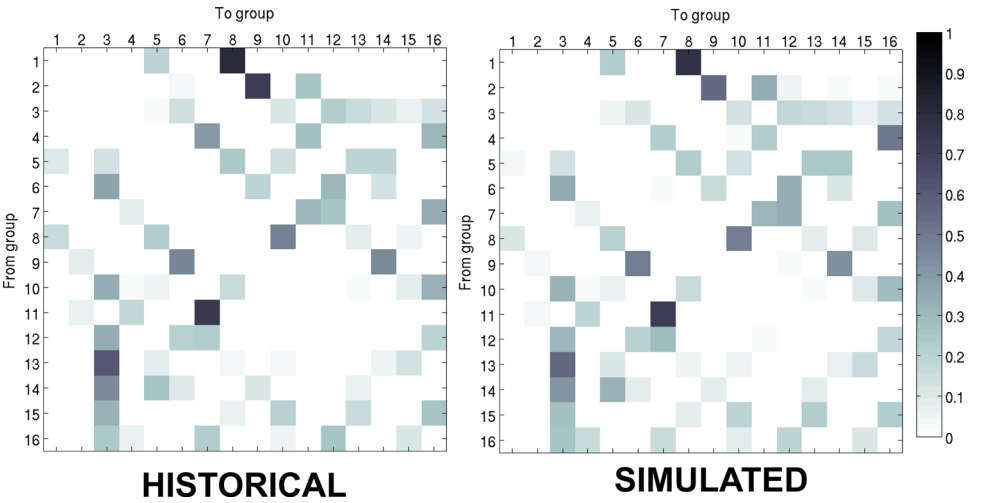

Figure 8. Comparison between (left) historical and (right) simulated total transition probabilities between clusters.

4.3.1. Maintaining the Probability of Occurrence

In long-term morphodynamic simulations, the characterization of the wave climate is critically important. Thus any synthetic series must reproduce "events" similar to historical ones. In terms of categorical series, the probability

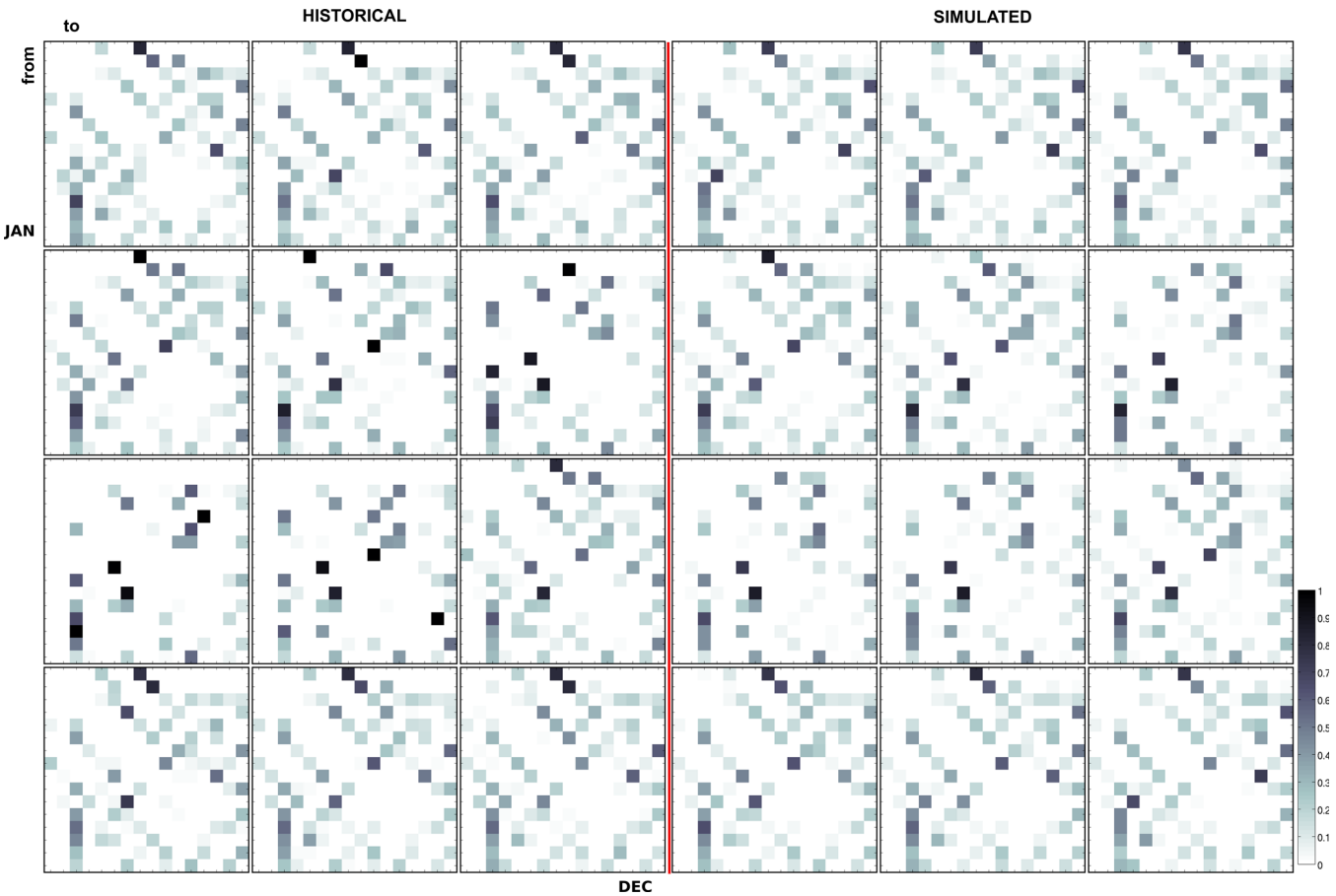

Figure 9. Monthly transition probability between clusters. (top, left) Matrix corresponds with January, and (bottom right) with December. The month increases from left to right and top to bottom (January, February, March; April, May, June; July, August, September; October, November, December). The historical matrices are plotted on the left side and the simulated matrices are plotted on the right side. Each matrix is defined following the cluster grouping as in Figure 8.

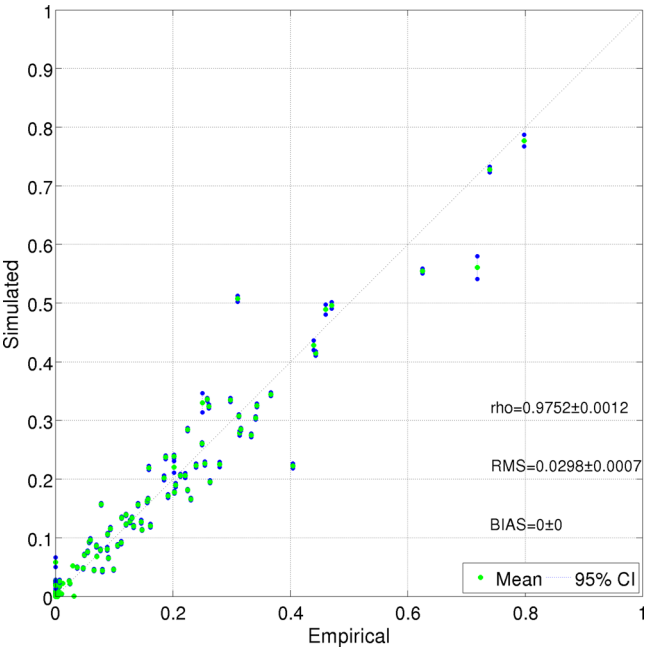

Figure 10. Comparison between historical (*x* axis) and simulated (*y* axis), total transition probabilities between clusters. Green dots represent mean values and blue ones represents 95% confidence intervals.

of occurrence of each SS must be equal. Figure 5 shows that seasonality is well reproduced over several years and Figure 6 demonstrates that the model is able to reproduce the seasonality over an average year with daily resolution.

Figure 7 illustrates the total occurrence probability of each cluster in the validation period (1990-2013) and reveals that the historical and simulated temporal series are consistent. The correlation coefficient between observed and simulated occurrence probability (ρ) is greater than 0.95, with a confidence interval $CI < \pm 0.005$, an unbiased population and *RMS* error lower than 2%.

4.3.2. Transition Probabilities

A key factor for wave input in long-term morphodynamics is the sequence of the different "events." Including patterns of wave chronology allows consideration of beach memory. Thus, the transition probability between SSs must be simulated properly.

Figure 8 compares the transition probabilities between clusters in a matrix layout, the correlation coefficient between observed and simulated transition probabilities ρ obtained exceeds 0.97 (CI $<\pm 0.0015$) and the *RMS* is lower than 3.0%. Figure 9 compares the observed and modeled monthly transition matrices. Here, ρ exceeds 0.85 ($CI < \pm 0.015$), the population is unbiased and the *RMS* is lower than 9%. Note that the diagonals in the matrices are empty. The probability of transition between the same SSs is zero and the persistence in the same group is obtained with the persistence model, e.g., equation (1).

Figure 10 illustrates the observed versus simulated total transition probabilities between clusters in the validation period (1990–2013). The correlation coefficient (ρ) exceeds 0.95, with a low confidence interval $CI < \pm 0.005$, an unbiased population and a *RMS* error lower than 2%.

4.3.3. Mean Energy Flux and Mean Energy Flux Direction

In this section, the wave energy flux (intensity and direction) are validated because of their importance in sediment transport calculations, as shown by *Mil-Homens et al.* [2013] and *van Rijn* [2014]. Furthermore, the transport of energy by ocean surface waves is crucial for the development of devices capturing wave power and in the estimation of the cost-efficiency of wave energy farms [*Reguero et al.*, 2015].

In our work, the Energy Flux (EF) is obtained from the wave spectral parameters using the expression:

$$EF = \frac{\rho g^2}{64\pi} T_{-10} H_s^2 \tag{4}$$

where T_{-10} is the energy period that is related with the spectral mean period, T_{01}, using $T_{-10} = \frac{m_{-1}}{m_0} = \alpha T_{01}$. Here, α is assumed to be 0.538 [*Reguero et al.*, 2015] and $T_{01} \approx T_{02}$.

As shown in Figures 11 and 12, the MUSCLE-morpho model correctly reproduces the total wave EF and the mean EF direction at seasonal scale and interannual scale, respectively. This result confirms that the MUSCLE-morpho emulator is able to reproduce the time-varying evolution of wave energy flux.

4.3.4. Morphological Application

Finally, we apply wave climate time series developed by MUSCLE-morpho to simulations of long-term morphodynamics. We perform comparisons of morphodynamic simulations using the nonlinear, implicit one-line model of *Vitousek and Barnard* [2015] and compare results produced with the real wave climate to the

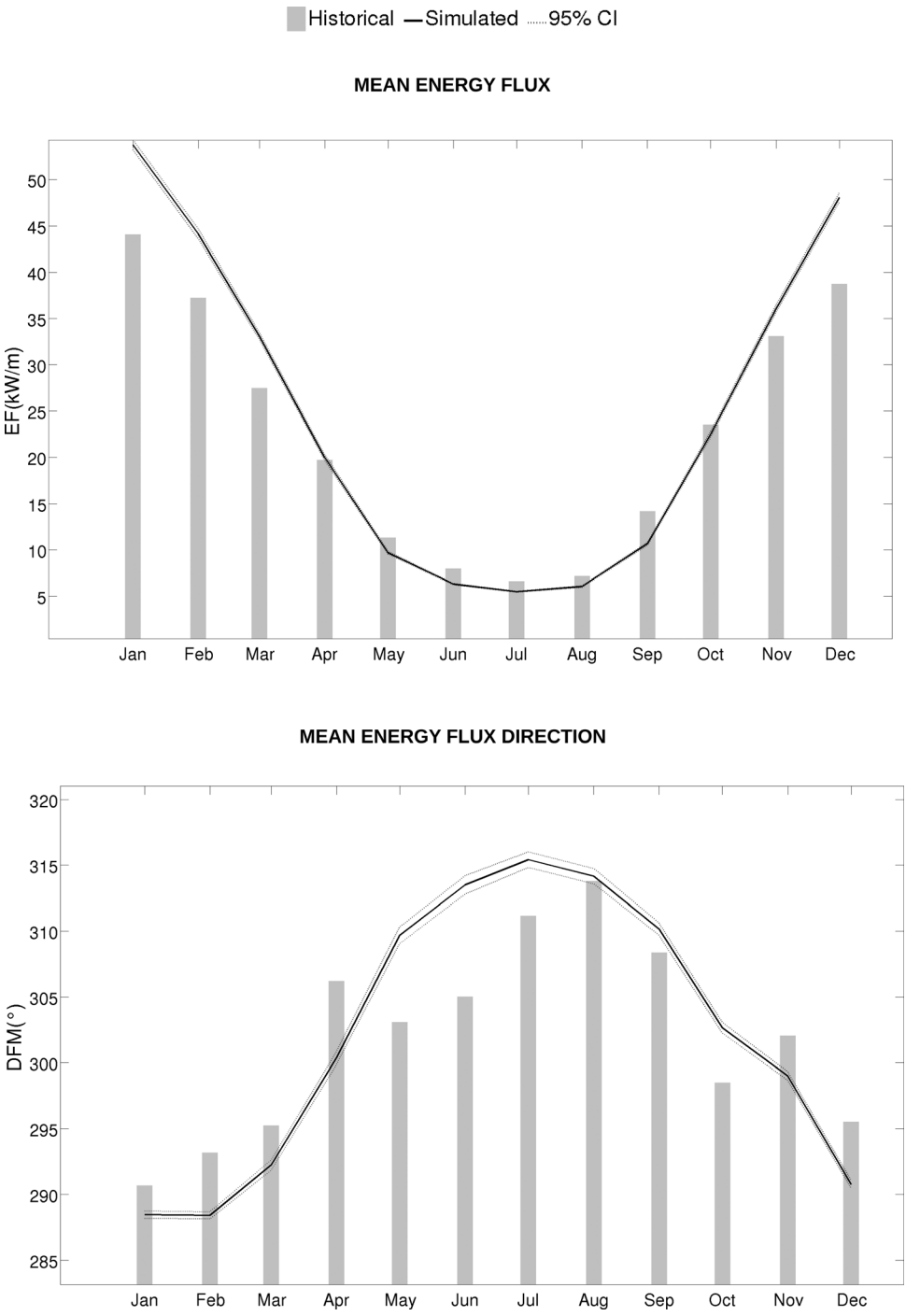

Figure 11. Comparison between historical (bars) and simulated (lines) (top) monthly mean energy flux and (bottom) monthly mean energy flux direction. Solid lines represent mean values, and dashed lines represent 95% confidence intervals.

simulated wave climate. Due to the implicit time-stepping procedure, the model is numerically stable for arbitrarily large time steps and, thus, is ideally suited to long-term simulations of shoreline change. The performance of the implicit model using input reduction is also compared against an explicit one-line model that simulates the complete time series.

Conservation of sediment in the alongshore direction neglecting cross-shore transport is the basis for the one-line shoreline model. The governing equation of the one-line model is given by

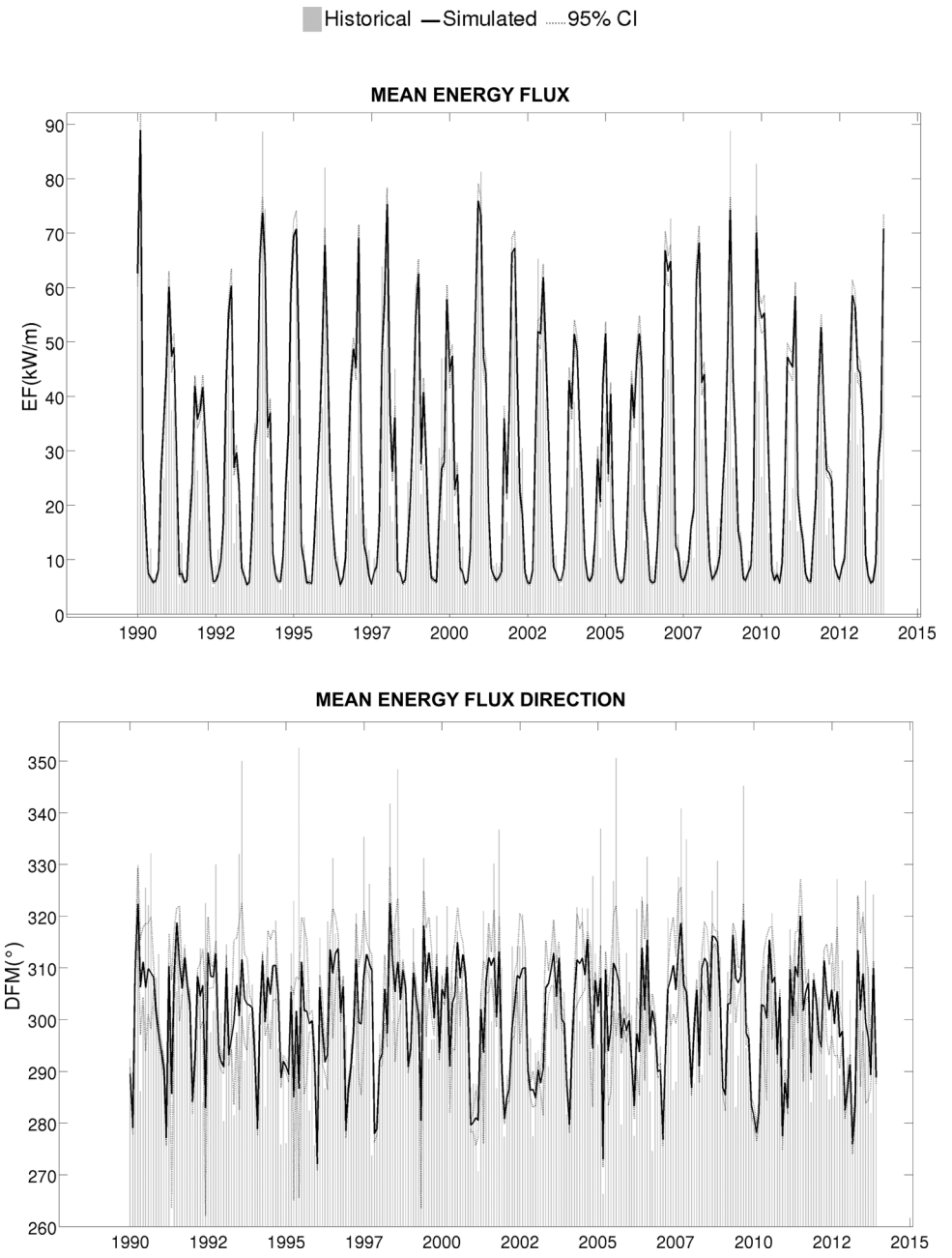

Figure 12. Comparison between historical (bars) and simulated (lines) (top) monthly mean energy flux through years and (bottom) monthly mean energy flux direction. Solid lines represent mean values, and dashed lines represent 95% confidence intervals.

$$\frac{\partial Y}{\partial t} = -\frac{1}{D_c}\frac{\partial Q}{\partial X}, \tag{5}$$

where Y is the cross-shore coordinate of the shoreline position, X is the alongshore coordinate, D_c is the depth of closure, Q is the longshore sediment transport rate, and t is time [*Larson and Kraus*, 1997]. Many one-line models are subject to a well-known physical instability in the presence of high angle waves [*Ashton and Murray*, 2006]. To reduce this instability, we split the typical alongshore sediment transport formula into nonlinear and linear transports according to

$$Q = Q_0\left[\theta_q \sin(2\alpha) - (1-\theta_q)2\frac{dy}{dx}\right], \tag{6}$$

Table 1. Run Times (Minutes: Seconds) for the Implicit and Explicit Models With the Simulated and Real Waves (SIMA, SIM, RIM, REX)

					Runtimes (Each Run)			
	Time Series	Model	Time Step	Runs	Mean	Max	Min	Speed Up
SIMA	Simulated	Implicit	Variable	100	00:9.30	00:9.87	00:8.81	~28
SIM	Simulated	Implicit	1 h	100	01:42.85	01:48.06	01:38.70	~2.5
RIM	Real	Implicit	1 h	1	01:40.88	01:40.88	01:40.88	~2.5
REX	Real	Explicit	50 s	1	04:12.84	04:12.84	04:12.84	1

where Q_0 represents the magnitude of the longshore transport rate, $\alpha = \alpha_{wave} - \alpha_{shoreline}$ represents the angle between the incident waves and the shoreline and the θ_q parameter weights the relative impact of the linear and nonlinear terms. Note that as waves become normally-incident, the linear and nonlinear transport terms in equation (6) become identical. The longshore transport rate Q_0, is given by the Shore Protection Manual [*SPM*, 1984], $Q_0 = \frac{\rho}{16} H_b C_{g,b} \frac{K}{(\rho_s - \rho)*\lambda}$, where ρ is the density of water, H_b is the breaking wave height, $C_{g,b}$ is the group velocity of the wave at breaking, K is an empirical constant, ρ_s is the sediment density, and λ is the porosity of the sediment. Here we assume $\rho = 1025$ kg/m^3, $\rho_s = 2650$ kg/m^3, $\lambda = 0.4$, and $K = 0.0098$.

We perform our numerical experiments along an idealized coastline of $L = 2$ km long with a shoreline orientation of $\alpha_{shoreline} = 200^\circ$ from the North (nautical convention), similar to the actual beaches in our study site (section 2). Boundary conditions are no flux ($Q = 0$) at the lateral boundaries, consequently embayed beach rotation driven by longshore sediment transport is essentially simulated. The model is run with $\theta_q = 0.7$ and $N = 80$ shoreline transects with $\triangle x = 25$ m grid spacing. The depth of closure is assumed to be $D_c = 15.5$ m following *Birkemeier* [1985].

The temporal discretization of the numerical method is varied for different model runs. We compare four different models, two using historical hindcast waves (as described in section 2.2, hereinafter referred to as Real) and two using the simulated waves obtained in section 4.2 for the period 1996–2006: (1) the first experiment, REX, simulates the Real wave time series (hourly hindcast) using the EXplicit model with a fixed time step of 50 s, (2) the second experiment, RIM, simulates the Real wave time series (hourly hindcast) using the IMplicit model with a fixed time step of 1 h, (3) the third experiment, SIM, simulates the Synthetic wave time series using the IMplicit model with a fixed time step of 1 h, (4) the fourth experiment, SIMA, simulates the Synthetic wave time series using the IMplicit model with a variable time step used to demonstrate MUSCLE-morpho's ability to "Accelerate" the morphodynamic simulations. Acceleration of each time step is related to the persistence of the wave climate given by the duration of the SS. Table 1 summarizes the features and execution times of the different numerical experiments described above.

Note that the variable time step in SIMA is linked with the relative energetic of various wave conditions, being higher with lower energy conditions and lower with higher energy conditions as determined by the persistence of the different SS clusters. Table 2 shows the minimum, mean, and maximum values of the Courant number in the different experiments. The implicit model allows significantly higher Courant numbers compared to the explicit model, and the synthetic time series enable the implicit model to develop its full potential in terms of efficiency.

Figure 13 illustrates one decade of shoreline evolution for the idealized coastal stretch for the four experiments, each reproducing the seasonal and interannual variability of the shoreline position. Results are

Table 2. Time Steps and Courant Numbers for the Implicit and Explicit Models With the Simulated and Real Waves (SIMA, SIM, RIM, REX)

					Courant Numbers		
	Time Series	Model	Time Steps	Runs	Min	Mean	Max
SIMA	Simulated	Implicit	4,544–5,068	100	0.37	55.13	2347.2
SIM	Simulated	Implicit	96,432	100	0.37	2.89	38.05
RIM	Real	Implicit	96,432	1	0.01	2.60	73.09
REX	Real	Explicit	6,943,033	1	0.00	0.04	1.00

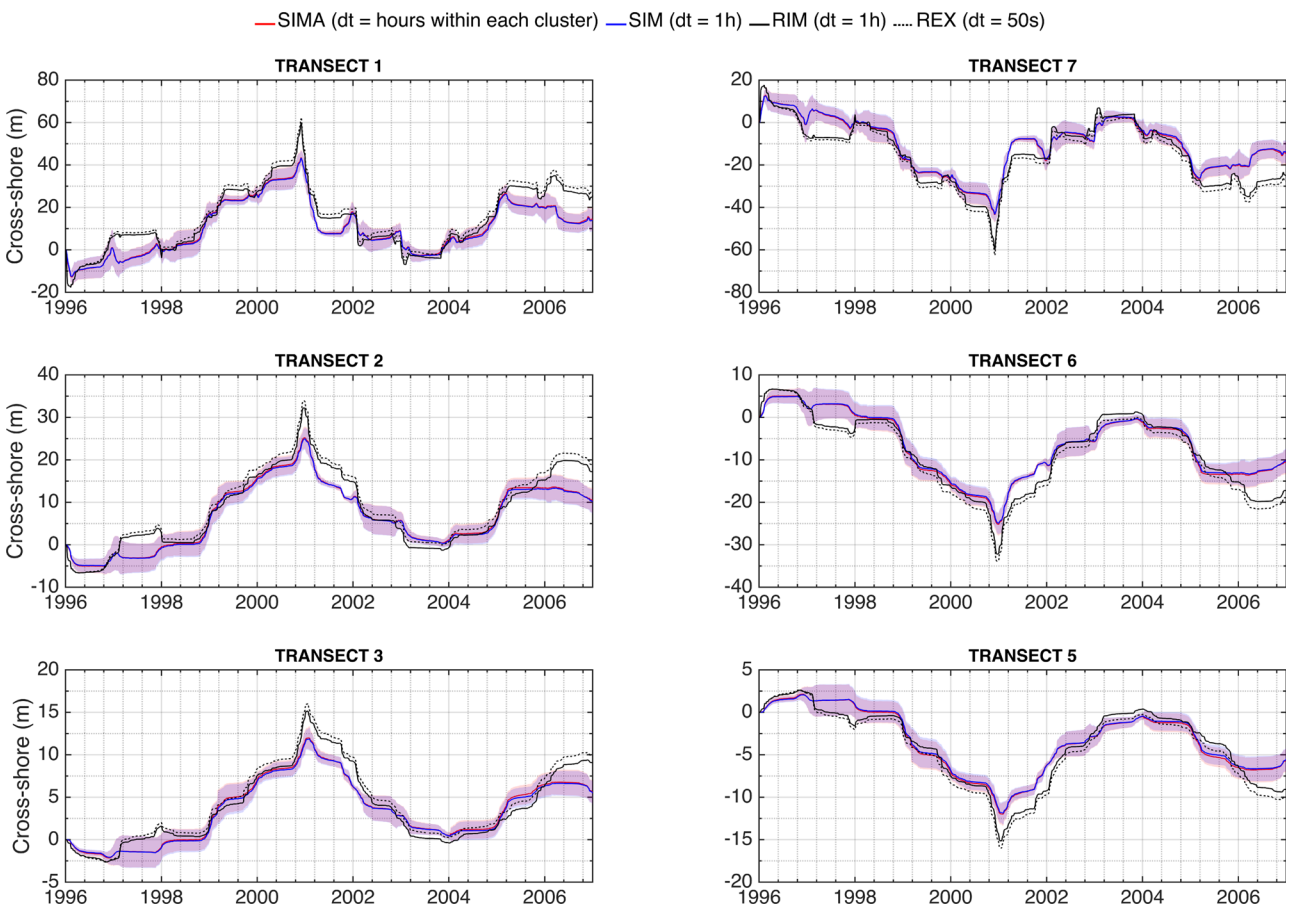

Figure 13. Shoreline evolution over a decade. For the simulated waves, the mean value of 100 simulations (solid line) and 95% confidence intervals (colored area) are represented.

shown at 250m spaced transects 1 to 7, from $x = -750$ m to $x = 750$ m, with the domain ranging from $x = -1000$ m to $x = 1000$ m.

The comparison between (1) REX and (2) RIM shows the performance of the explicit method against the implicit method (Figure 13). The implicit method reduces the execution time by a factor of three while maintaining the behavior of the shoreline evolution. Comparing (1) REX or (2) RIM against (3) SIM, validates that the input-reduced time series given by MUSCLE-morpho produces consistent long-term morphological behavior. Figure 13 demonstrates that the synthetic time series retains the seasonal and interannual response of the shoreline over a decade. The comparison between (3) SIM and (4) SIMA in Table 1 demonstrates that using the MUSCLE-morpho synthetic time series reduces the computational time by several orders of magnitude, even in a relatively simple one-line modeling framework.

This numerical experiment demonstrates that the model is ready to reproduce the morphological evolution over a range of different time scales (seasonal, interannual, and beyond). The methods presented here are ideally suited to ensemble prediction, and thus provide a basis for a highly efficient probabilistic shoreline change modeling framework. In this particular application, we have forced the model to follow the historical evolution of the daily SLP fields. Further research will be needed to couple this model with a stochastic model for time series of daily SLP fields [*Guanche et al*., 2013].

5. Conclusions

The MUSCLE-morpho model allows for the generation of synthetic time series of the multivariate wave climate accounting for past characteristics. The approach can generate long-term multivariate time series of sea state parameters (wave height, period, and direction) taking into account many scales of variability (seasonal, interannual) that affect long-term (decadal and beyond) morphodynamics. The MUSCLE-morpho

model can also be used to generate future wave climate time series and account for possible changes in the global climate system by means of changes in the covariates (e.g., SLP fields). This method can also capture long-term changes in persistence and event sequence of the wave climate. Efficient prediction of the long-term wave climate is vital to modeling long-term morphodynamics. Furthermore, probabilistic, ensemble-prediction methods will become increasingly important as we further develop the range of possible climate change scenarios. The MUSCLE-morpho modeling system, described here, represents an input reduction tool to drive the next generation of morphodynamic models.

Acknowledgments

José Antonio A. Antolínez is indebted to the MEC (Ministerio de Educación, Cultura y Deporte, Spain) for the funding provided in the FPU (Formación del Profesorado Universitario) studentship (BOE-A-2013-12235). J. A. A. Antolínez, F. J. Méndez, and E. M. González acknowledge the support of the Spanish "Ministerio de Economia y Competitividad" under Grant BIA2014-59643-R. This material is based upon work supported by the U.S. Geological Survey under Grant/Cooperative Agreement G15AC00426. The work has been partially funded by project "2013/S 122-208379—Assessment of climate impacts on coastal systems in Europe" from the European Commission, JRC, Institute for Prospective Technological Studies (IPTS). Wave data from Global Ocean Waves (GOW) database could be requested to Environmental Hydraulics Institute at email address: ihdata@ihcantabria.com. NCEP reanalysis data are provided by the NOAA/OAR/ESRL PSD, Boulder, Colorado, USA, from their Web site at http://www.esrl.noaa.gov/psd/.

References

Ashton, A. D., and a. B. Murray (2006), High-angle wave instability and emergent shoreline shapes: 1. Modeling of sand waves, flying spits, and capes, *J. Geophys. Res.*, *111*, F04011, doi:10.1029/2005JF000422.

Birkemeier, W. a. (1985), Field data on seaward limit of profile change, *J. Waterw. Port Coastal Ocean Eng.*, *111*(3), 598–602, doi:10.1061/(ASCE)0733-950X(1985)111:3(598).

Caires, S., V. R. Swail, and X. L. Wang (2006), Projection and analysis of extreme wave climate, *J. Clim.*, *19*(21), 5581–5605, doi:10.1175/JCLI3918.1.

Callaghan, D. P., P. Nielsen, A. Short, and R. Ranasinghe (2008), Statistical simulation of wave climate and extreme beach erosion, *Coastal Eng.*, *55*(5), 375–390, doi:10.1016/j.coastaleng.2007.12.003.

Callaghan, D. P., R. Ranasinghe, and D. Roelvink (2013), Probabilistic estimation of storm erosion using analytical, semi-empirical, and process based storm erosion models, *Coastal Eng.*, *82*, 64–75, doi:10.1016/j.coastaleng.2013.08.007.

Camus, P., F. J. Mendez, R. Medina, and A. S. Cofiño (2011), Analysis of clustering and selection algorithms for the study of multivariate wave climate, *Coastal Eng.*, *58*(6), 453–462, doi:10.1016/j.coastaleng.2011.02.003.

Camus, P., M. Menéndez, F. J. Méndez, C. Izaguirre, A. Espejo, V. Cánovas, J. Pérez, A. Rueda, I. J. Losada, and R. Medina (2014a), A weather-type statistical downscaling framework for ocean wave climate, *J. Geophys. Res. Oceans*, *119*, 7389–7405, doi:10.1002/2014JC010141.

Camus, P., F. J. Méndez, I. Losada, M. Menéndez, A. Espejo, J. Pérez, A. Rueda, and Y. Guanche (2014b), A method for finding the optimal predictor indices for local wave climate conditions, *Ocean Dyn.*, *64*(7), 1025–1038, doi:10.1007/s10236-014-0737-2.

Casas-Prat, M., X. L. Wang, and J. P. Sierra (2014), A physical-based statistical method for modeling ocean wave heights, *Ocean Modell.*, *73*, 59–75, doi:10.1016/j.ocemod.2013.10.008.

Chesher, T., and G. Miles (1992), *The Concept of a Single Representative Wave for Use in Numerical Models of Long Term Sediment Transport Predictions*, Ashgate Publ., Aldershot.

Chonwattana, S., S. Weesakul, and S. Vongvisessomjai (2005), 3D Modeling of morphological changes using representative waves, *Coastal Eng. J.*, *47*(4), 205–229, doi:10.1142/S0578563405001240.

de Vriend, H., M. Capobianco, T. Chesher, H. de Swart, B. Latteux, and M. Stive (1993a), Approaches to long-term modelling of coastal morphology: A review, *Coastal Eng.*, *21*(1–3), 225–269, doi:10.1016/0378-3839(93)90051-9.

de Vriend, H., J. Zyserman, J. Nicholson, J. Roelvink, P. Péchon, and H. Southgate (1993b), Medium-term 2DH coastal area modelling, *Coastal Eng.*, *21*(1–3), 193–224, doi:10.1016/0378-3839(93)90050-I.

Elko, N., et al. (2014), The future of nearshore processes research, Abstract OS22A-08 presented at 2014 Fall Meeting, AGU, San Francisco, Calif., December.

Gōda, Y. (2010), Random seas and design of maritime structures, *in Advanced Series on Ocean Engineering*, edited by P. L. F. Liu, World Sci., Singapore.

Griggs, G. B. (2013), Lost neighborhoods of the California coast, *J. Coastal Res.*, *299*, 129–147, doi:10.2112/13A-00007.1.

Guanche, Y., R. Mínguez, and F. J. Méndez (2013), Autoregressive logistic regression applied to atmospheric circulation patterns, *Clim. Dyn.*, *42*(1–2), 537–552, doi:10.1007/s00382-013-1690-3.

IPCC (2013), *Climate Change 2013: The Physical Science Basis. Contribution of Working Group I to the Fifth Assessment Report of the Intergovernmental Panel on Climate Change*, p. 33115, Cambridge Univ. Press, Cambridge, doi:10.1017/CBO9781107415324.005.

Kaergaard, K., and J. r. Fredsoe (2013), Numerical modeling of shoreline undulations part 2: Varying wave climate and comparison with observations, *Coastal Eng.*, *75*, 77–90, doi:10.1016/j.coastaleng.2012.11.003.

Kalnay, E., et al. (1996), The NCEP/NCAR 40-year reanalysis project, *Bull. Am. Meteorol. Soc.*, *77*(3), 437–471, doi:10.1175/1520-0477(1996)077<0437:TNYRP>2.0.CO;2.

Kistler, R., et al. (2001), The NCEPNCAR 50 year reanalysis: Monthly means CDROM and documentation, *Bull. Am. Meteorol. Soc.*, *82*(2), 247–267, doi:10.1175/1520-0477(2001)082<0247:TNNYRM>2.3.CO;2.

Latteux, B. (1995), Techniques for long-term morphological simulation under tidal action, *Mar. Geol.*, *126*(1–4), 129–141, doi:10.1016/0025-3227(95)00069-B.

Larson, H. H., M., and N. Kraus (1997), Analytical solutions of one-line model for shoreline change near coastal structures, *J. Waterw., Port Coastal Ocean Eng.*, *123*(4), 180–191, doi:10.1061/(ASCE)0733-950X(1997)123:4(180).

Lesser, G. R. (2009), An approach to medium-term coastal morphological modelling, PhD thesis, Delft Univ. of Technol., Netherlands.

Menéndez, M., F. J. Méndez, C. Izaguirre, A. Luceño, and I. J. Losada (2009), The influence of seasonality on estimating return values of significant wave height, *Coastal Eng.*, *56*(3), 211–219, doi:10.1016/j.coastaleng.2008.07.004.

Menendez, M., M. García-Díez, L. Fita, J. Fernández, F. J. Méndez, and J. M. Gutiérrez (2013), High-resolution sea wind hindcasts over the Mediterranean area, *Clim. Dyn.*, *42*(7–8), 1857–1872, doi:10.1007/s00382-013-1912-8.

Mil-Homens, J. a., R. Ranasinghe, J. van Thiel de Vries, and M. Stive (2013), Re-evaluation and improvement of three commonly used bulk longshore sediment transport formulas, *Coastal Eng.*, *75*, 29–39, doi:10.1016/j.coastaleng.2013.01.004.

Mínguez, R., F. J. Méndez, C. Izaguirre, M. Menéndez, and I. J. Losada (2010), Pseudo-optimal parameter selection of non-stationary generalized extreme value models for environmental variables, *Environ. Modell. Software*, *25*(12), 1592–1607, doi:10.1016/j.envsoft.2010.05.008.

Nicholls, R. J., and A. Cazenave (2010), Sea level rise and its impact on coastal zones, *Science*, *328*(2010), 1517–1520, doi:10.1126/science.1185782.

Norris, J. R. (1997a), Continuous-time Markov chains I, in *Markov Chains*, edited by J. R. Norris, pp. 60–107, Cambridge Univ. Press, Cambridge.

Norris, J. R. (1997b), Continuous-time Markov chains II, in *Markov Chains*, edited by J. R. Norris, pp. 108–127, Cambridge Univ. Press, Cambridge.

Pérez, J., F. J. Méndez, M. Menéndez, and I. J. Losada (2014a), Estela: A method for evaluating the source and travel time of the wave energy reaching a local area, *Ocean Dyn.*, *64*(8), 1181–1191, doi:10.1007/s10236-014-0740-7.
Pérez, J., M. Menendez, F. J. Mendez, and I. J. Losada (2014b), Evaluating the performance of CMIP3 and CMIP5 global climate models over the north-east Atlantic region, *Clim. Dyn.*, *43*(9–10), 2663–2680, doi:10.1007/s00382-014-2078-8.
Pérez, J., M. Menendez, P. Camus, F. J. Mendez, and I. J. Losada (2015), Statistical multi-model climate projections of surface ocean waves in Europe, waves and coastal, regional and global processes, *Ocean Modell.*, *96*, Part 1, 161–170, doi:10.1016/j.ocemod.2015.06.001.
Reguero, B., M. Menéndez, F. Méndez, R. Mínguez, and I. Losada (2012), A Global Ocean Wave (GOW) calibrated reanalysis from 1948 onwards, *Coastal Eng.*, *65*, 38–55, doi:10.1016/j.coastaleng.2012.03.003.
Reguero, B. G., I. J. Losada, and F. J. Méndez (2015), A global wave power resource and its seasonal, interannual and long-term variability, *Appl. Energy*, *148*, 366–380, doi:10.1016/j.apenergy.2015.03.114.
Roelvink, J. (2006), Coastal morphodynamic evolution techniques, *Coastal Eng.*, *53*(2-3), 277–287, doi:10.1016/j.coastaleng.2005.10.015.
Salvadori, G., G. Tomasicchio, and F. D'Alessandro (2014), Practical guidelines for multivariate analysis and design in coastal and off-shore engineering, *Coastal Eng.*, *88*, 1–14, doi:10.1016/j.coastaleng.2014.01.011.
Southgate, H. N. (1995), The effects of wave chronology on medium and long term coastal morphology, *Coastal Eng.*, *26*(3-4), 251–270, doi:10.1016/0378-3839(95)00028-3.
SPM (1984), *U S. Army Corps of Engineers, Shore Protection Manual*, vol. 2, 37–53 pp., Army Eng. Waterw. Exp. Stn., Vicksburg, Miss.
Steijn, R. (1992), Input filtering techniques for complex morphological models, in *H: Waterloopkundig Laboratorium*, vol. 824, edited by R. Steijn, Delft Hydraul. Lab., Netherlands.
Thomsen, K., and P. Sørensen (1999), Fatigue loads for wind turbines operating in wakes, *J. Wind Eng. Ind. Aerodyn.*, *80*(1-2), 121–136, doi:10.1016/S0167-6105(98)00194-9.
van Rijn, L. C. (2014), A simple general expression for longshore transport of sand, gravel and shingle, *Coastal Eng.*, *90*, 23–39, doi:10.1016/j.coastaleng.2014.04.008.
Vitousek, S., and P. L. Barnard (2015), A nonlinear, implicit one-line model to predict long-term shoreline change, in *Coastal Sediments 2015*, edited by P. Wang, J. D. Rosati, and J. Cheng, chap. 215, World Sci., Singapore.
Walstra, D. J. R., R. Hoekstra, P. K. Tonnon, and B. G. Ruessink (2013), Input reduction for long-term morphodynamic simulations in wave-dominated coastal settings, *Coastal Eng.*, *77*(0), 57–70, doi:10.1016/j.coastaleng.2013.02.001.
Wang, X. L., Y. Feng, and V. R. Swail (2012), North Atlantic wave height trends as reconstructed from the 20th century reanalysis, *Geophys. Res. Lett.*, *39*, L18705, doi:10.1029/2012GL053381.
Zhang, K., B. C. Douglas, and S. P. Leatherman (2004), Global warming and coastal erosion, *Clim. Change*, *64*, 41–58.

Erratum

In the originally published version of this article, the first author's name was presented incorrectly as Jose Antonio A. Álvarez. This has been corrected to read José Antonio A. Antolínez, and this version may be considered the authoritative version of record.